Received: 17 May 2017 | Accepted: 6 December 2017

DOI: 10.1002/hyp.11424

RESEARCH ARTICLE

WILEY

Complex patterns of catchment solute–discharge relationships for coastal plain rivers

Jacob S. Diamond[1] | Matthew J. Cohen[2]

[1] School of Forest Resources and Environmental Conservation, Virginia Tech, Blacksburg, VA, USA

[2] School of Forest Resources and Conservation, University of Florida, Gainesville, FL, USA

Correspondence
Jacob S. Diamond, School of Forest Resources and Environmental Conservation, Virginia Tech, Blacksburg, VA, USA.
Email: jacdia@vt.edu

Funding information
National Institute of Food and Agriculture, Grant/Award Number: FLA-FOR-005284; Florida Forest Service; National Council for Air and Stream Improvement

Abstract

Riverine solute versus discharge (C–Q) relationships provide information about the magnitude and dynamics of material fluxes from landscapes. We analysed long-term patterns of C–Q relationships for 44 rivers in Florida across a suite of geogenic, nutrient, and organic solutes and investigated land cover, watershed size, and surficial geology as controls on these patterns. Solute concentrations generally exhibited far less variability than did discharge, with coherent solute-specific behaviours repeated across watersheds. Geogenic solutes generally diluted with increasing discharge, whereas organic solutes generally enriched; patterns for nutrients were highly variable across watersheds, but on average exhibited chemostasis. Despite strong evidence of both geologic and land cover controls on solute flow-weighted concentrations, these variables were poor predictors of C–Q slopes (β) or relative coefficients of variation (CV_C:CV_Q). CV_C:CV_Q generally increased with watershed size, and wetland area appeared to influence C–Q patterns for base cations and organic solutes. Perhaps most importantly, we observed significant slope breaks in C–Q association in approximately half of our observations, challenging the generality of using single power functions to describe catchment solute export patterns. For all solutes except phosphorus (P), C–Q slopes decreased above statistically identified breaks (slopes for P increased), with breaks consistently at or near median flow (i.e., 50% flow exceedance probability). This common pattern significantly impacts solute load estimates; failing to account for slope breaks overestimates nitrate and total organic carbon loads as much as 125% and underestimates P loads as much as 35%. In addition to challenging generic power-law characterization of C–Q relationships for these coastal plain rivers, and exploring the load estimate consequences thereof, our study supports emerging insights about watershed hydrochemical behaviours across a wide array of solutes.

KEYWORDS

chemostasis, concentration, C–Q, Florida, watershed

1 | INTRODUCTION

Streamflow and its associated chemical fluxes are the filtered integration of hydrologic and biogeochemical processes in a watershed. As such, the study of hydrochemical fluxes helps resolve questions regarding watershed-scale structure and function (Feng, Kirchner, & Neal, 2004; Kirchner, Feng, Neal, & Robson, 2004). In addition to helping reveal catchment and landscape processes, an understanding of stream and solute dynamics in catchments is vital for water management decisions in which the magnitude of and controls on chemical fluxes, as well as ecosystem responses to those fluxes, are needed. For example, recent work on nutrient fluxes to the Gulf of Mexico from the Mississippi River Basin reveals complex temporal dynamics that affect load assessments (Pellerin et al., 2014). More broadly, setting water quality standards for lakes, streams, rivers and, estuaries is predicated on understanding contaminant loads, which are, in turn, estimated from associations between streamflow and chemical fluxes. A long legacy of efforts to interpret concentration–discharge (C–Q) relationships has informed critical watershed processes (e.g., Evans & Davies, 1998, Godsey, Kirchner, & Chow, 2009, Johnson & Likens, 1969). For example, streamflow concentrations of some geogenic solutes (e.g., Na^+ and Si^{4+}) decrease with increasing discharge, implying dilution effects (Clow & Drever, 1996; Johnson & Likens, 1969), and inference of solute source limitation. In contrast, some solute concentrations increase with increasing discharge (e.g., Al^{3+},

dissolved and particulate organic carbon), possibly due to increasing source area contribution, and implying solute transport limitation (Herndon et al., 2015b). Other solutes (e.g., Mg^{2+}, Ca^{2+}, Cl^{-}, and NO_3^{-}) are highly buffered (i.e., exhibit low variation in concentration with respect to discharge; Basu, Thompson, & Rao, 2011, Stallard & Murphy, 2014, Herndon et al., 2015b). This variation across solutes is attributed to both watershed-scale phenomena such as biological uptake (Mulholland & Hill, 1997), mixing between sources (Seibert et al., 2009; Stallard & Murphy, 2014), and point-scale reaction rate equilibria between soil water and weathered bedrock (Anderson, Dietrich, Torres, Montgomery, & Loague, 1997; Godsey et al., 2009).

Most early work on C–Q relationships in streams focused on event-scale dynamics (Evans & Davies, 1998; Johnson & Likens, 1969), but recent studies drawing on long-term data synthesis have highlighted the importance of interannual patterns in solute transport (Basu et al., 2010; Godsey et al., 2009). Despite evidence for event-scale solute dilution effects, analysis over longer time scales reveals pervasive chemostasis—defined as low variation in concentration despite large variation in discharge—across many watersheds (10^1–10^6 km^2) and for numerous solutes (Basu et al., 2010; Basu et al., 2011; Godsey et al., 2009; Guan et al., 2011).

Chemostatic behaviour may arise from solute supply sufficient to exceed transport capacity (Basu et al., 2010; Godsey et al., 2010; Murphy, Hornberger, & Liddle, 2012), although other mixing-model explanations have been advanced (e.g., Kim, Dietrich, Thurnhoffer, Bishop, & Fung, 2017). Flow, or transport, limitation may occur when watersheds with a large source mass of solute, because of either significant geogenic sources or legacy anthropogenic loading, buffer hydrologic variation to yield concentrations that are constant with respect to flow. Similarly, chemostasis may also arise where water residence times are long compared to solute equilibrium times, such that there is always sufficient time for equilibrium between bedrock and groundwater. However, Godsey et al. (2009) point out that for some geogenic solutes (e.g., Si^{4+}), equilibrium reaction rates are far slower than water transit times, implying that streamwater is always far from solute equilibrium. For such reaction-limited solutes, the C–Q relationship should be dominated by dilution. Dilution effects may be mitigated by the presence of a homogeneously distributed, ubiquitous source mass, such that all groundwater flowpaths sample a similar distribution of solid phase minerals.

Other solute concentrations increase (i.e., become enriched) with increasing discharge, suggesting that event-water mobilizes solutes that are otherwise unavailable to streamflow during base-flow periods. This could occur by the episodic connectivity of near-surface and surficial pathways with which these solutes are associated. This behaviour has been observed for dissolved organic solutes derived from surficial organic deposits, which are mobilized by connecting new flow generating locations to the stream network (Bishop, Seibert, Kohler, & Laudon, 2004; Herndon et al., 2015a; Herndon et al., 2015b).

Several key questions emerge from the recent literature. First, what controls variation in C–Q patterns across catchments and solutes? Although there have been tentative explanations invoking land use intensity, lithology, and size, a systematic understanding of controls remains a knowledge gap. Second, how general are power-function descriptions of C–Q associations across watersheds and solutes? Most previous work has utilized a simple power function to characterize C–Q relationships (i.e., $C = \alpha Q^{\beta}$). Under chemostatic conditions, C collapses to a constant (α) as the slope (β) goes to zero, such that load is directly flow proportional ($L = aQ$). This linear relationship between flow and load has important implications for predicting chemical fluxes to receiving water bodies (Basu et al., 2010; Jawitz & Mitchell, 2011). Despite the ubiquity of simple power functions to describe the C–Q association, recent work (Moatar, Abbott, Minaudo, Curie, & Pinay, 2017) has questioned that generality, with strong evidence of discrete breaks in the C–Q association slope that have important load estimation implications.

In this work, we explored three aspects of catchment C–Q relationships using long-term data synthesized from rivers of varying size in Florida. First, we investigated patterns of catchment delivery across a suite of solutes, ranging from those principally under geologic (e.g., Si, Ca, Mg, and pH) or evaporative (e.g., Cl and Na) control to those principally under biological control (e.g., total organic carbon [TOC] and total Kjeldahl nitrogen [TKN]), as well as those most likely to be influenced by anthropogenic activities (e.g., P and N). On the basis of previous work, we expected all solutes to vary less than discharge, but we hypothesized that solute variation would exhibit coherent patterns across widely variable catchments for specific solutes. We predicted consistent dilution behaviour for geogenic solutes, chemostatic behaviour for evaporative solutes, enrichment behaviour for organic solutes, and mixed behaviours for solutes under significant human influence.

Second, we examined controls on specific solute C–Q variation across catchments. We hypothesized that C–Q relationships vary in response to watershed land cover, size, and lithology. Although Godsey et al. (2009) found minimal effect of these controls on C–Q relationships, we surmised that our regional approach would isolate these controls by reducing variability in climate and topography. Specifically, we predicted larger watersheds, which filter small-scale variability in solute source mass and distribution, will exhibit greater chemostasis for all solutes. Further, we predicted that lithology—in particular, the prevalence of exposed carbonates versus siliciclastics—controls geogenic solutes, resulting in chemostasis for solutes associated with each dominant rock type (e.g., chemostasis for Ca^{2+} in limestone areas). Similarly, we predicted that land use, in particular wetlands and urban/agricultural lands, exerts strong controls on organic and nutrient solute signals, respectively.

Our third area of inquiry pertained to the generality of simple power functions to depict C–Q associations across solutes and watersheds. The compelling contrary findings of non-linearities in log(C)–log(Q) space described by Moatar et al. (2017) prompted our prediction that power-function slope breaks are common features of C–Q relationships in these coastal plain catchments. We sought to characterize the prevalence and magnitude of such slope breaks, assess their coherence across solutes and flow conditions, and quantify their impact for solute load estimates.

2 | METHODS

2.1 | Site selection and data screening

We synthesized monitoring data for streams and rivers in northern peninsular Florida, in the southeastern coastal plain of the United

States. The region—starting north of Lake Okeechobee to omit complex anthropogenic drainage features of extreme southern Florida, and east of the Apalachicola River, omitting the influence of drainage from other physiographic settings—is characterized by low relief, abundant rainfall, variable land cover, and two major geologic domains, including Pleistocene siliciclastic and Eocene carbonate lithologies.

We obtained most solute concentration data from the Storage and Retrieval (STORET) database maintained by the Florida Department of Environmental Protection, which archives the extensive monitoring of physical, chemical, and biological attributes of Florida's waters over the past ~30 years. We obtained additional data from the United States Geological Survey (USGS) National Water-Quality Assessment Program. We chose sites according to the following criteria: (a) on a stream or river and (b) at least five continuous years of concentration data records. These criteria reduced the number of study sites from ~20,000 in all of STORET to ~200, most of which were second-order rivers or larger. We selected the following solutes on the basis of data availability and management relevance: nitrate plus nitrite (NO_3), pH, TKN, total phosphorus (TP), phosphate (PO_4), specific conductance (SpC), silica (Si), sodium (Na), chloride (Cl), calcium (Ca), magnesium (Mg), and TOC.

We obtained discharge data, which are unavailable in STORET, from USGS National Water Information System (NWIS), queried for all daily river flow records in the study domain. To concatenate concentration and flow records, we matched STORET and NWIS stations if the scalar distance between them was below 100 m; stations without a match were discarded. The number of matched stations was insensitive to the 100-m cut-off distance, with no additional matched stations until distances between STORET and NWIS stations were over 1,000 m, which we considered too distant for this analysis. This matching process reduced the number of sites to ~100. We then matched flow data to water quality data by day of sampling. At all sites, there were sampling dates where streamflow chemistry was missing for solutes of interest; some sites had no observations for certain solutes. Further site refinement eliminated site C–Q relationships with fewer than 50 dates with both flow and chemistry data. This criterion ensured adequate time coverage for most C–Q relationships (e.g., 5 years at monthly sampling), while providing enough data points for robust power-law analysis (Clauset, Shalizi, & Newman, 2009). Because 80% of the omitted C–Q relationships had 36 observations or less, lowering the 50 sample threshold had limited impact on site numbers. The final selection criterion eliminated sites with significant influence from tides, control structures (e.g., dams and canals), and point source discharges (e.g., wastewater treatment plants). This screening process identified 44 sites for detailed analysis.

We further screened available data by eliminating individual water quality observations with the following comments (database code in parentheses): off-scale low (K), off-scale high (L), sample held beyond accepted holding time (Q), value reported less than laboratory detection limit (T), value reported above detection limit (V), sample improperly preserved (Y), and other nonstandard comments that suggested the observation was either inaccurate or unusable. Data losses from this screening were substantial (~30% at some sites). However, when we compared solute concentration distributions before and after this step, we found them to be nearly identical (i.e., ratio of means and standard deviations before and after screening = 1), indicating no major loss of information. After screening, 25% of sites fell below the 50 sample threshold but were all retained for our analysis.

To evaluate whether screened dates represent the range of flow conditions, we compared flow on dates with water chemistry samples to the entire flow record at each site. We conducted a Kolmogorov–Smirnov test for each site to test the null hypothesis that flow distributions for dates with chemistry data were drawn from the same distribution as the entire site record. We also conducted a Wilcoxon rank-sum test for each site to test the null hypothesis that a randomly selected flow value from dates with chemistry data is different from a randomly selected value from the entire flow distribution. We were unable to reject the null hypotheses for either test at $p = .01$ for 42 out of 45 sites, indicating that our data are generally representative of the site flow regime. At three sites where the rank-sum test suggested a significant mismatch between flow with and without solute measurements (USGS gages, p value: 02312600, .005; 02294898, .003; 02320700, .002), the observed histogram mismatch was sufficiently small for us to conclude that their inclusion does not compromise our results. For every site, the distribution of flows for dates with water chemistry data truncated the overall flow distribution. This is expected, particularly at extreme flow values, where sampling can be dangerous.

Water quality data are coarse resolution (mostly monthly, some quarterly). At all sites, SpC was the most frequently measured parameter (usually monthly). Dissolved oxygen and temperature were both also frequently sampled but were not included in our analysis because they vary systematically both seasonally and diurnally. We did not exclude other solutes that may exhibit diel signals (Kurz, de Montety, Martin, Cohen, & Foster, 2013) but acknowledge that sampling time-of-day may affect our results. We did not correct solute concentrations for precipitation chemistry because concentrations for all solutes are generally orders of magnitude higher in streamflow (Godsey et al., 2009). Because of data resolution limits, we did not index solute measurements by hydrograph position, season, or antecedent rainfall.

2.2 | Watershed data processing

For each site, we obtained watershed hydrologic unit codes (HUCs; Watershed Boundary Dataset 2012). HUC level varied across sites, and some included multiple HUCs; roughly half were HUC-12 (10^1–10^2 km^2), with the rest HUC-10 (10^2–10^3 km^2). From the HUCs, we obtained total watershed area, drainage density, and location of the sampling station with respect to the watershed outlet. Drainage areas ranged from 17.4 to 24,320 km^2 (median = 504 km^2). We obtained annual runoff data from USGS station reports, literature values (USGS 1995), and, if neither was available, direct calculations. Mean annual runoff varied from 4.0 to 71.1 cm year^{-1} (median = 28.1 cm year^{-1}). The period of record for all sites ranged from 5 to 31 years (median = 12 years).

We obtained land use data from the Florida Land Use, Cover and Forms Classification System, which is publicly available from the Florida Fish and Wildlife Conservation Commission (http://myfwc.com/research/gis/applications/articles/fl-land-cover-classification). We aggregated Florida Land Use, Cover and Forms Classification

System classes to wetlands, urban, and agricultural lands and quantified the fractional coverage of each within each HUC. Although land cover is dynamic, our analysis considered conditions only in 2008 or 2010, depending on the site. Generally, land cover was 10–50% forests and wetlands, with some basins with up to 40–50% agricultural cover (mainly in southwest Florida). We performed all spatial calculations in ArcGIS v. 9.0 (ESRI, Redlands, CA).

Stratigraphy/lithology maps from Florida Department of Environmental Protection (http://www.dep.state.fl.us/gis/datadir.htm) were intersected with HUC boundaries to determine the underlying geology at each site. Formations of interest included the Miocene Hawthorn Group, an important confining unit in the study region and above which Pleistocene siliciclastics dominate, and Eocene Ocala limestone, which is the formation that contains the upper Floridan aquifer, and which consists of nearly pure carbonate rock with occasional dolostone inclusions. The Ocala is at or near the surface in the west-central and north-central portions of Florida where it exhibits extensive karstification. This karst drainage network significantly impacts regional hydrology, with numerous large artesian springs fed by karst conduits contributing substantially to river flows. The Hawthorn Group varies in thickness and composition throughout the study domain. Generally, it consists of interbedded siliciclastic materials and low permeability carbonate clays with high phosphate content.

2.3 | Concentration–discharge analysis

We calculated site-specific coefficients of variation for concentrations (CV_C) and discharge (CV_Q), their ratio (CV_C:CV_Q), and flow-weighted concentrations (FWCs) for each solute. The CV_C:CV_Q is recently used as an indicator for export regime (Musolff, Fleckenstein, Rao, & Jawitz, 2017; Thompson, Basu, Lascurain, Aubeneau, & Rao, 2011), with values less than 0.5 indicating chemostasis (Musolff et al., 2017). The FWC allows us to test landscape and lithologic controls on magnitudes of solute delivery, irrespective of concentration variation. To further evaluate C–Q relationships, we initially fitted a linear model to the relationship between log-transformed solute concentrations (except pH, which is already log scaled and was analysed untransformed) and log-transformed daily discharge using iteratively reweighted least squares to reduce outlier influence. We then extracted the fitted slopes (β) as well as their 95% confidence intervals, the coefficients of determination (R^2), and model residuals. We tested linear regression assumptions by plotting residuals and applying the Breusch–Pagan test for homoscedasticity. Unless otherwise stated, we conducted all analyses using R (R Core Team, 2016).

2.4 | Breakpoint analysis

Many C–Q relationships appeared non-linear in log–log space, often visually better represented by piecewise linear fits versus the widely used single power function (Godsey et al., 2009; Smith, Chambers, & Hollibaugh, 1996; Thompson et al., 2011). We applied a breakpoint analysis to all log(C)–log(Q) relationships, starting with a Davies test on each linear model fit using the *segmented* package in R (Vito & Muggeo, 2003, 2008) to test the null hypothesis of a constant linear predictor (β in this case) for each site and solute. The Davies test uses k quantiles (k = 10 in this case) of the predictor variable distribution for breakpoints in the linear relationship and computes Wald statistics for the difference-in-slope at each of these k breakpoints. It then selects the minimum p value from these difference-in-slope tests at each quantile breakpoint. When the Davies test null hypothesis was rejected ($p < .05$), we conducted breakpoint analysis to estimate the fit for a model with two slopes, precluding consideration of models with more than one breakpoint (e.g., three slopes) or other non-linear fits. Our model did not specify breakpoint values a priori but instead optimized each breakpoint location by iteratively fitting standard iteratively reweighted least squares models, which minimize the influence of outliers on slope estimation. We constrained each model so that at least 15% of the data were on either side of the breakpoint to avoid extreme flow or concentration influences.

We extracted the specific discharge values (mm day^{-1}; volumetric discharge divided by watershed area) at each breakpoint, the associated discharge exceedance probability, and C–Q regression parameters on each side of the breakpoint. Finally, we evaluated regression slopes (β) before and after a breakpoint to assess systematic variation in the size and direction of observed changes across solutes and watersheds, and for comparisons of predicted solute mass loading between C–Q models using one versus two slopes.

2.5 | Watershed analysis

We correlated CV_C:CV_Q, fitted β values, and FWCs with land use (i.e., % cover of urban, agricultural, forests, or wetlands), lithology (i.e., % cover of Hawthorn and Ocala formations), and watershed size. We used the Spearman rank correlation (ρ) for these pairwise relationships because we could not assume linear relationships. This pairwise analysis yielded 21 regressions per solute and 252 relationships over the entire dataset. Because many sites did not have any exposed Ocala or Hawthorn, we also conducted a pairwise test for presence versus absence of these features. We conducted both two-sample t tests and two-sample Mann–Whitney U tests (to account for nonnormality and to compare with t tests) assuming unequal variances for the following solute-specific relationships: (a) presence or absence of Hawthorn Group versus CV_C:CV_Q for PO_4, (b) presence or absence of Hawthorn Group versus FWC for PO_4, (c) presence or absence of limestone versus CV_C:CV_Q for Ca, and (d) presence or absence of limestone versus FWC for Ca. Site geology was binary based on presence (1) or absence (0) of a formation in the contributing watershed; presence was designated where a formation covered at least 1% of the drainage area.

3 | RESULTS

3.1 | Patterns of C–Q relationships

C–Q plots (i.e., log[C] vs. log[Q]) suggest predominant power-law behaviour for solutes across study watersheds (Figure 1). However, 31% of the C–Q relationships did not meet constant variance assumptions, and an additional 23% were poorly fitted by simple power-law functions (Table 1). The most frequently heteroscedastic solutes were pH, NO_3, and SpC. Nonsignificant slopes were most common for TP/PO_4, Cl, and NO_3, whereas the poorest fits (low R^2) were observed

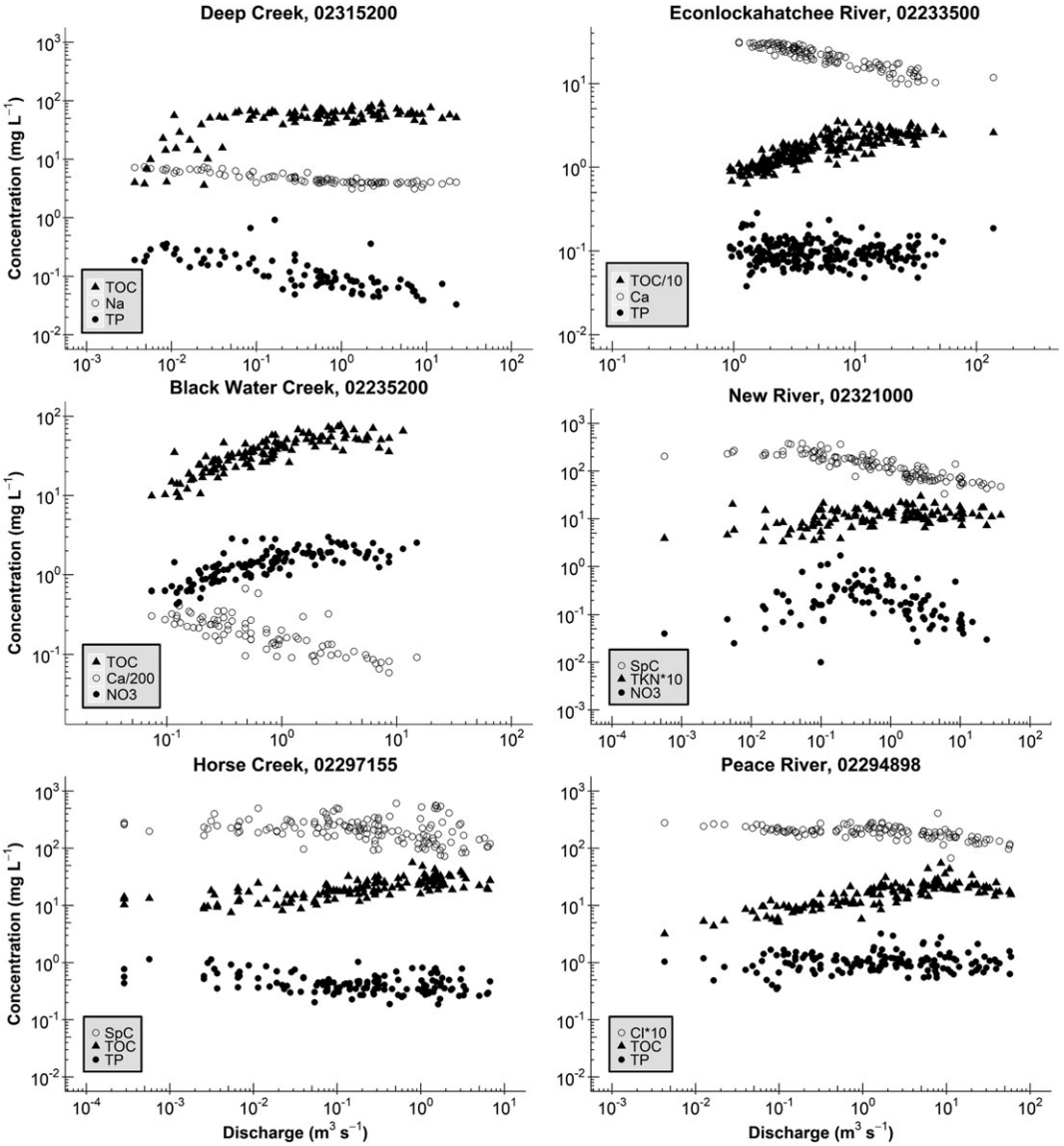

FIGURE 1 C–Q relationships for selected sites and solutes plotted on logarithmic axes. River names and associated United States Geological Survey gage numbers at the top of each plot. Each plot contains an instance of three main solute types analysed in this study (nutrients, geogenics, or evaporative, and organics). Notice general small variations in concentration despite large variations in discharge. Further notice scaling breaks in organic solute C–Q relationships (triangles) at all sites, and the NO_3 scaling break for the New River site at approximately 0.2 $m^3\ s^{-1}$. SpC = specific conductance; TKN = total Kjeldahl nitrogen; TOC = total organic carbon; TP = total phosphorus

TABLE 1 Statistical evaluation of all 443 C–Q relationships in this study

Test parameter	Percentage of total C–Q relationships	Notes
Not homoscedastic	31	Breusch–Pagan test with $p < .05$
β not significant	18	$p > .05$
Not homoscedastic and β not significant	3	See above
Low R^2 and β not 0[a]	3	$R^2 < .20$ (weighted)
Low R^2 and β not 0[a]	23	$R^2 < .20$ (unweighted)

[a]β not 0 defined as $|\beta| > 0.05$.

for NO_3, PO_4, and TKN. Across sites, Mg and Ca dynamics exhibited the best fit to single power-function behaviour, whereas TP, PO_4, and NO_3 exhibited the worst fits (Figure 1).

Consistent patterns emerged for all solutes across watersheds (Figure 2a). Cation solutes (Ca and Mg), generally of geogenic origin, exhibited consistent damped dilution with increasing discharge (interquartile range [IQR] for β_{Ca} = −0.4 to −0.2 and β_{Mg} = −0.6 to −0.2), with Ca and Mg exhibiting nearly identical behaviours. Similarly, we note that FWCs of Mg and Ca were highly correlated, with Ca consistently 1.5–2 times higher than Mg. SpC and pH had similar β ranges to geogenic cations, but evaporative solutes (Cl and Na) were more chemostatic (IQR for β_{Cl} = −0.2 to −0.0 and β_{Na} = −0.3 to −0.0). FWCs for Cl and Na were highly correlated, with Cl concentrations consistently twice as high as Na, suggesting similar solute enrichment and delivery processes. We observed enrichment for organic solutes, especially for TOC (IQR = 0.1–0.5). C–Q relationships for nutrients (NO_3, PO_4, TP, and TKN) varied between enrichment, chemostasis, and dilution. These varied relationships were similar among nutrients, but PO_4 and TP exhibited greater chemostasis (IQR = −0.1 to 0.1), whereas C–Q

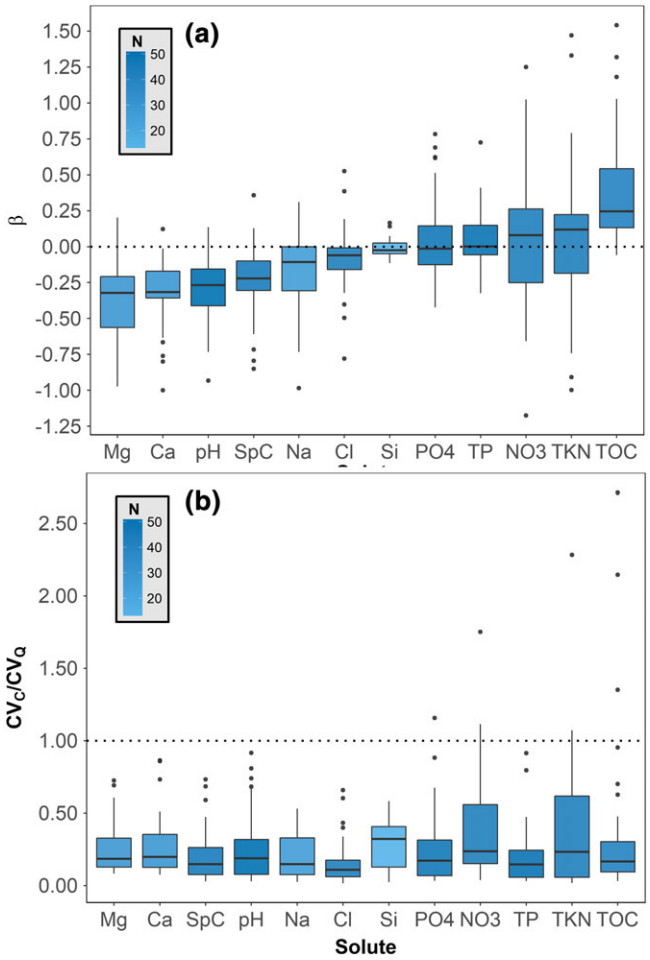

FIGURE 2 (a) Ranking of log(C)–log(Q) β values, averaged across sites; error bars are standard deviations. Geogenic solutes have the most negative β values, organic solutes the most positive, and nutrients the most variable. For this analysis, we note here that when breakpoints are present in a C–Q relationship, we present the β that comprises the majority of the flow distribution. Breakpoint here is defined as the flow that separates a simple linear log(C)–log(Q) relationship into a piecewise log(C)–log(Q) relationship. For example, if a breakpoint was found at a flow exceedance probability of 30%, we would present the β from the second linear segment, which comprises 70% of the flow distribution. (b) Ranking of CV_C:CV_Q, averaged across sites; there are no error bars. Standard boxplots are colored by the number (N) of C-Q relationships for each solute. SpC = specific conductance; TKN = total Kjeldahl nitrogen; TOC = total organic carbon; TP = total phosphorus

associations for NO_3 (IQR = −0.3 to 0.3) and TKN (IQR = −0.2 to 0.2) varied over a much broader range. FWCs for TP and NO_3 were uncorrelated, with flow-weighted TP concentrations varying far less (~50%) than NO_3. Although Si data were limited because of site screening criteria, Si exhibited near-chemostatic behaviour across all sites.

Calculated CVs indicate that although C–Q relationships can be enriching, diluting, or chemostatic, most solutes exhibited much less variability in concentration (CV_C = 0.1–3.3) than did flow (CV_Q = 0.3–32.2). Contrasting solute and discharge variation using CV_C:CV_Q revealed that all solute concentrations vary substantially less than did discharge (mean CV_C:CV_Q = 0.27 ± 0.30, n = 435; Figure 2b), underscoring the primacy of flow variation in enumerating solute loads.

3.2 | Controls on C–Q relationships

3.2.1 | Lithology

We observed significant lithologic control on C–Q associations. The Hawthorn and Ocala formations were present in 57% and 32% of sites, respectively, with 30% containing both. Presence of the Hawthorn, an economically important source of P, was correlated with decreased CV_C:CV_Q and increased FWCs for PO_4 (Table 2). Similarly, presence of the Ocala was correlated with increased FWCs for Ca but, in contrast to the impact of Hawthorn on PO_4, was associated with increased CV_C:CV_Q for Ca (p < .01). As with Ca, we observed a positive correlation between Ocala cover and FWCs for Mg (Table 2). Indeed, positive correlation with Ocala cover and CV_C:CV_Q was evident for nearly all solutes (Table 3). In contrast, a strong negative correlation between Hawthorn cover and CV_C:CV_Q was observed for nearly all solutes (Table 3). We observed no significant correlations between lithology and fitted slopes (β values), except for TP/PO_4 and limestone, where increasing Ocala cover led to higher β values (Table 3).

3.2.2 | Watershed size

Watershed size was not strongly or significantly correlated with C–Q β or FWC values. However, watershed size was consistently positively correlated to CV_C:CV_Q for every solute, and these correlations were significant for most geogenic and evaporative solutes and TP/PO_4 (Table 4).

3.2.3 | Land cover

Overall, land cover was slightly more correlated with C–Q β values than was watershed size for all solutes, but the direction and strength of correlation were solute dependent (Table 4). The most compelling land cover controls on β values were inverse correlations between wetlands and Ca and Mg, and forests and pH. Some broader trends were evident, however, with pH exhibiting greater dilution with

TABLE 2 Results from two-sample t tests and Mann–Whitney tests for differences in mean CV_C:CV_Q and FWCs for phosphate and calcium among sites with differing lithologies

	CV_C:CV_Q		FWC (mg L^{-1})	
	Present	**Absent**	**Present**	**Absent**
PO_4				
Hawthorn Group				
Mean	0.24	0.33	0.22	0.076
Variance	0.072	0.044	0.052	0.0059
Observations	16	25	16	25
t statistic; W statistic	−1.19; 119		2.82; 308	
p ($T \le t$); p ($W \le w$)	.12; **.015**		**.0040**; **.0016**	
Ca				
Ocala				
Mean	0.42	0.18	29.53	11.38
Variance	0.069	0.011	85.05	277.07
Observations	12	17	12	17
t statistic; W statistic	2.99; 167		3.42; 174	
p ($T \le t$); p ($W \le w$)	.995; .999		**.0018**; **.00045**	

Note. FWC = flow-weighted concentration. Bold p values indicate significance at p<0.05.

TABLE 3 Spearman correlation coefficients (ρ) for geologic controls on solute–discharge relationships

	Ocala			Hawthorn		
Solute	β	FWC	CV_C:CV_Q	β	FWC	CV_C:CV_Q
Ca	−0.15	**0.57****	**0.43***	−0.03	−0.21	−0.27
Cl	0.01	0.06	0.21	0.15	**−0.39***	**−0.45****
Mg	−0.37	**0.62*****	**0.52****	0.07	−0.27	−0.34
Na	−0.12	0.16	**0.48***	**0.46***	**−0.64*****	**−0.57****
NO_3	0.28	0.08	0.12	−0.06	**−0.40****	0.06
pH	−0.16	0.26	**0.30***	0.18	0.08	**−0.48*****
PO_4	**0.54*****	**−0.33***	**0.49*****	0.14	0.56*****	**−0.52*****
Si	0.22	−0.22	0.55	−0.21	0.26	**−0.64***
SpC	−0.13	**0.36***	**0.36***	0.14	−0.09	**−0.33***
TKN	0.07	**−0.33***	**0.58*****	**0.43****	**0.45****	**−0.45****
TOC	0.27	−0.16	**0.32***	−0.05	0.05	**−0.33***
TP	**0.58*****	**−0.32***	**0.43****	0.20	**0.53*****	**−0.50*****

Note. In the case of a piecewise regression, the β values used here are the β values that comprise the majority of data points in the relationship. SpC = specific conductance; TKN = total Kjeldahl nitrogen; TOC = total organic carbon; TP = total phosphorus.

*$p < .05$.

**$p < .01$.

***$p < .001$.

increased wetland and forest cover, but enrichment with greater urban cover. We also observed that increasing wetland cover generally increased dilution for many solutes, although this relationship was only significant for Ca, Mg, pH, and TOC. Although not obvious from Spearman correlation coefficients in Table 4, we observed greater urban cover associated with chemostasis (i.e., β = 0) for several solutes (i.e., Ca, Mg, Na, pH, SpC, and TP). This convergence on chemostasis was nonmonotonic, becoming apparent only for urban cover above 30%, which applied to only five sites.

Land cover controls on CV_C:CV_Q were not consistent, though we did observe some notable patterns. Increasing forest cover was negatively associated with CV_C:CV_Q for geogenic and evaporative solutes, but positively associated with CV_C:CV_Q for pH and nutrients (Table 4). Increasing urban cover exhibited the opposite signal, where CV_C:CV_Q increased for nearly every solute, although the correlations were weaker than for forest cover.

Land cover was much more strongly and significantly correlated with solute FWC, especially for forest cover (Table 4). Interestingly, wetlands and forests exhibited similar inverse correlations with FWC values for every solute except TOC, which had the opposite relationship (Table 4). In contrast, agriculture cover and urban cover were associated with higher FWC values for most solutes (except TOC; Table 4). Wetlands had the strongest and most significant correlations with FWC values of Si and TOC (ρ = −0.73 and 0.51); agriculture was most associated with SpC, TKN, and TP (ρ = 0.44, 0.41, and 0.41); forests with SpC and TP/PO_4 (ρ = −0.64 and −0.58); and urban cover with Na and Ca (ρ = 0.82 and 0.60).

3.3 | Breakpoints

Breakpoints in C–Q relationships were present for at least one solute in every river, and each catchment exhibited a mean breakpoint flow exceedance probability of 50% (normally distributed with mean = 0.5 and standard deviation = 0.2). Two-slope models were a better representation than the one-slope model for approximately 50% of all C–Q relationships. Solutes most likely to exhibit two-slope behaviour were Cl, SpC, Ca, TOC, Na, and Mg, for which 60–70% of watersheds exhibited significant breakpoints (Figure 3). Solutes least likely to exhibit two-slope behaviour were Si, TP, and PO_4, for which 20–30% of watersheds exhibited significant breakpoints. There was no clear pattern in site characteristics to predict breakpoints, but at some sites

TABLE 4 Spearman correlation coefficients (ρ) for land cover controls on solute–discharge relationships

	Watershed area[a]			Percentage wetland			Percentage forest			Percentage agricultural			Percentage urban		
Solute	β	FWC	CV_C:CV_Q	β	FWC	CV_C:CV_Q	β	FWC	CV_C:CV_Q	β	FWC	CV_C:CV_Q	β	FWC	CV_C:CV_Q
Ca	−0.35	0.18	**0.48****	**−0.50****	−0.27	0.20	0.02	**−0.47***	−0.33	−0.19	0.30	0.32	0.33	**0.60*****	0.06
Cl	0.09	−0.29	0.27	0.00	−0.20	−0.17	**0.33***	**−0.52*****	−0.12	−0.20	0.11	0.03	−0.11	**0.52*****	**0.39***
Mg	−0.36	0.26	**0.49****	**−0.53****	−0.13	0.27	0.10	**−0.44***	**−0.45***	−0.26	**0.42***	0.34	0.17	**0.46***	0.17
Na	−0.32	−0.13	**0.48***	−0.15	−0.31	−0.12	0.24	**−0.46***	**−0.53****	**−0.41***	0.15	**0.55****	−0.24	**0.82*****	**0.62*****
NO_3	−0.16	−0.10	0.28	−0.15	−0.29	**−0.33***	0.15	−0.06	−0.02	−0.17	−0.11	**0.38***	**0.32***	**0.49*****	0.00
pH	**−0.29***	0.17	**0.30***	**−0.40****	**−0.36***	0.20	**−0.54*****	**−0.50*****	**0.41****	0.23	0.21	−0.18	**0.47*****	**0.56*****	−0.06
PO_4	0.16	−0.12	**0.38****	0.09	**−0.37***	0.13	−0.18	**−0.58*****	**0.35***	**0.30***	**0.36***	−0.03	0.17	0.10	0.09
Si	−0.20	0.04	0.46	−0.24	**−0.73****	0.13	−0.09	0.52	**−0.66***	0.45	0.26	0.47	0.22	0.17	**0.58***
SpC	−0.20	0.05	**0.46****	0.08	−0.03	−0.04	−0.18	**−0.64*****	0.03	−0.14	**0.44****	0.20	−0.10	**0.34***	0.26
TKN	**0.38***	0.02	0.22	−0.14	−0.10	0.09	−0.01	**−0.51*****	**0.40****	**0.31***	**0.41****	−0.22	−0.29	−0.24	0.15
TOC	0.12	−0.11	0.23	**−0.36***	**0.51*****	−0.24	**0.31***	**0.35***	0.28	−0.08	−0.25	−0.13	0.26	**−0.48****	**0.38***
TP	0.18	−0.08	**0.29***	−0.02	**−0.43****	0.07	−0.25	**−0.58*****	**0.29***	**0.42****	**0.41****	−0.08	0.09	0.12	0.10

Note. In the case of a piecewise regression, the β values used here are the β values that comprise the majority of data points in the relationship. SpC = specific conductance; TKN = total Kjeldahl nitrogen; TOC = total organic carbon; TP = total phosphorus.

[a]Results are presented using the natural log of watershed area versus solute–discharge relationship variables.

*$p < .05$.

**$p < .01$.

***$p < .001$.

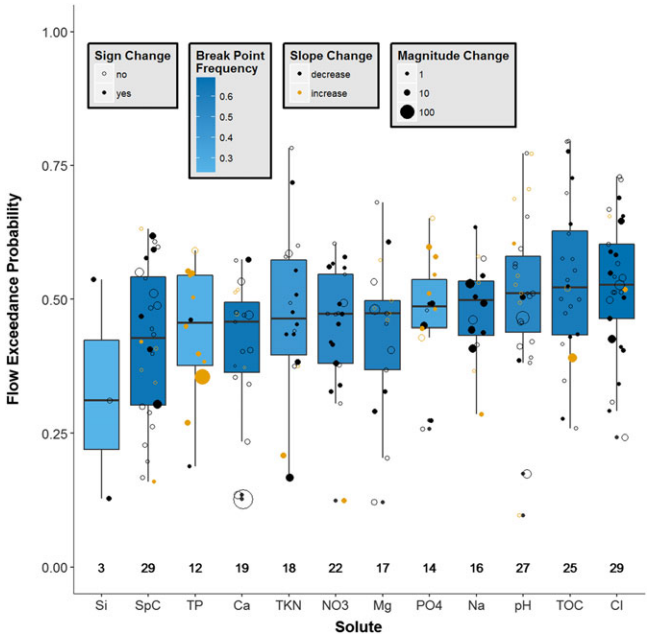

FIGURE 3 Flow exceedance probability of slope break by solute across basins. Boxes are filled by the frequency of C–Q relationships for that solute that had slope breaks (e.g., close to 70% of sites with measured Cl data had breakpoints in their C–Q relationship). Points are closed if there was a sign change in the C–Q slope at the breakpoint. Yellow symbols indicate that the slope steepened, and black symbols indicate that it became more shallow (or closer to chemostatic). Thus, if a point is filled in and black, then it had a positive C–Q slope before the breakpoint and a negative one after. The size of a point indicates how big of a change in slope magnitude was observed at the slope break. Numbers along the bottom row indicate total number of slope breaks by solute across all sites. Most breakpoints for solutes are centred on an exceedance probability of 50%. SpC = specific conductance; TKN = total Kjeldahl nitrogen; TOC = total organic carbon; TP = total phosphorus

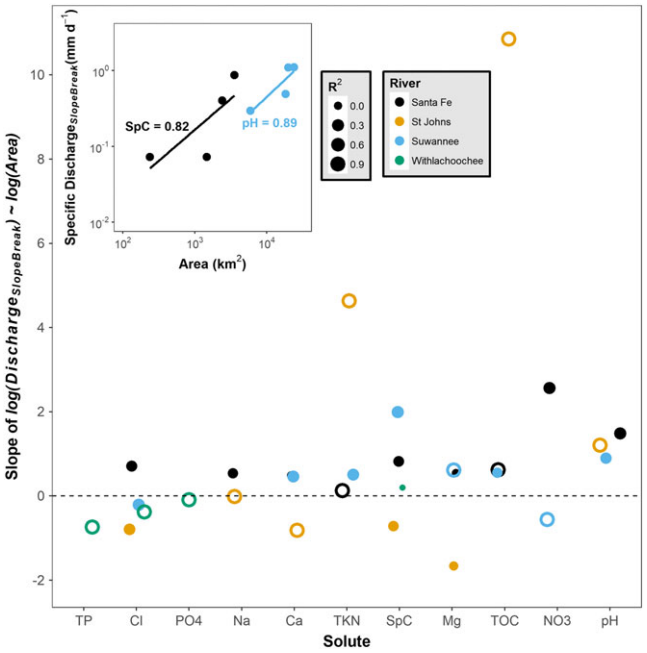

FIGURE 4 Slope of the relationship between the discharge (mm day $^{-1}$) at which the slope break occurred and the watershed area for each solute along four rivers in Florida. Both discharge and area are log transformed before regression. Points are coloured by their river and sized by the R^2 value of their relationship. Points are open if they only had 2 points in the relationship. Inset shows two example slope calculations for pH at the Suwannee River and SpC at the Santa Fe River. There tends to be an increase in flow depth at which flow breaks occur for these rivers, but there is no universal trend. SpC = specific conductance; TKN = total Kjeldahl nitrogen; TOC = total organic carbon; TP = total phosphorus

(e.g., Santa Fe River, 02321975; and Horse Creek, 02297310) over 90% of solutes exhibited breakpoints.

Estimated breakpoints centred on approximately median flow (i.e., flow exceedance probability of 0.5; Figure 3). Moreover, breakpoints for all solutes within a watershed tended to be at the same flow, suggesting activation of transient flowpaths at high discharge. In most cases (77%), power-function slopes (β values) decreased above the breakpoint (Figure 3; black vs. gold). Increases in β were less common (23%) and consistently observed only for TP. Fitted slopes changed sign in 40% of catchments (Figure 3; open vs. closed), particularly for nutrients (TP, PO_4, NO_3, and TKN). Finally, slope changes above each breakpoint were generally small (Figure 3; size of points), though in some important examples, large changes in slope were observed (e.g., for TP, pH, and SpC). The mean slope below the breakpoint indicated chemostasis (mean = 0), whereas above the breakpoint, modest dilution was most common (mean = −0.2).

Longitudinal patterns in breakpoint behaviours from multiple stations at different network positions were available in four basins (Figure 4). Although the relationship between breakpoint specific discharge and watershed size (from different network positions; Figure 4, inset) varied substantially across solutes, we observed a potentially important pattern. Specifically, larger basins tend to exhibit slope breaks at substantially greater specific discharge (Q), particularly for pH, SpC, TOC, and TKN; slopes of log(Q) versus log(A) were generally around 1, suggesting that each log-unit increase in area increases the specific discharge breakpoint by 1 log-unit. As such, the generic observation of breakpoints at median flow appears to be watershed size dependent.

4 | DISCUSSION

Our results support the generality of catchment solute chemostasis across a wide suite of solutes. In all cases, solute concentrations varied markedly less than did discharge, and power-function slope magnitudes (|β|) between C and Q were almost always below 1. Generic chemostasis is of basic interest because it guides development and evaluation of hydrologic models, though several mechanisms can explain such behaviour (e.g., Godsey et al., 2009; Li et al., 2017; Seibert et al., 2009). It is also of practical interest because chemostasis simplifies solute load calculations by focusing attention on flow as the dominant driver of variation in downstream loading. We further report that solutes with different sources and functions (e.g., geogenic vs. organic vs. nutrient solutes) behave differently, but with strong similarities across catchments, suggesting consistent source generation and transport processes despite considerable variation in lithology, land cover, and size. Although catchment size or land cover controls on

C–Q relationships were weak, some promising avenues of further work emerged. Perhaps most importantly, our regional results do not provide support for the presumed generality of single power functions to describe solute–discharge relationships. Indeed, we observed distinct C–Q slope breakpoints and thus marked improvement of model fit when adopting a two-component power function, with important implications for load estimates. Slope breaks are common, the breakpoints generally reduce β values, and they occur at or near median discharge. Together, these imply source activation and flowpath dynamics that are likely relevant to an emerging understanding of catchment functions.

4.1 | Commonality and complexity in C–Q relationships

Our results strongly support the hypothesis that solute concentrations vary less than discharge. Less than 3% of the 443 unique C–Q relationships had concentration variation equal to or greater than discharge variation (i.e., CV_C:$CV_Q \geq 1$), and 86% had CV_C:CV_Q below 0.5. Moreover, most (56%) C–Q relationships had $|\beta| < 0.2$, a threshold for designating chemostasis (Li et al., 2017). This provides strong local support, under low relief conditions, for the general contention that mixing damps solute variation across catchment storages and flowpaths even where those flowpaths rapidly mobilize stored water following rain events (Beven, 2010; Botter, Bertuzzo, & Rinaldo, 2010; Pearce, Stewart, & Sklash, 1986).

C–Q patterns support the prediction that individual solutes behave similarly across catchments. Geogenic solutes (Ca, Mg, and Si) generally exhibited weak dilution (i.e., slightly negative β), a result widely observed for streams and rivers (Basu et al., 2010; Godsey et al., 2009; Johnson & Likens, 1969; Meybeck & Moatar, 2012; Musolff, Schmidt, Selle, & Fleckenstein, 2015). Our results add pH to the list of solutes exhibiting weak dilution power-law behaviour with discharge, suggesting high flows activate new sources of acidity, likely as a result of CO_2 (and attendant carbonic acid) enrichment from organic matter respiration in the soil, vadose zone, and shallow groundwater.

Silica was the most chemostatic solute, implying a large source mass mobilized equally at all flows, likely a result of quartz minerals dominating regional surficial sediments. In contrast, consistent shallow negative β values for base cations (e.g., calcium and magnesium) indicate different mobilization and transport processes. The carbonate minerals (e.g., calcite and dolomite) that are the likely source of base cations have dissolution rates five orders of magnitude greater than those of quartz (Brantley, 2008; Nangia & Garrison, 2008). This appears to contradict predictions from a coupled weathering and transport model (Ameli et al., 2016) that as the ratio of equilibrium concentration to maximum dissolution rate decreases, C–Q approaches chemostasis. We observed that solutes with smaller ratios of equilibrium concentration to maximum dissolution rates (i.e., calcium and magnesium) exhibit greater dilution than did those with larger ratios (i.e., silica). We suggest that biotic mechanisms may help reconcile these observations. Silica can be a significant component of terrestrial biomass (e.g., some species contain up to 10–15% of silica in dry shoot weight; Epstein, 1994, Conley, 2002), and studies have shown that biogenic silica release is twice that of silica release due to silicate mineral weathering (Alexandre, Meunier, Colin, & Koud, 1997). Moreover, because most biogenic silica is collocated with soil organic carbon, it represents a rapidly mobilizable source of silica sampled at high flows. In that conceptualization, enrichment effects from biogenic sources may counterbalance dilution effects from geogenic sources.

Similar to silica, evaporative solutes (Cl and Na) were clearly chemostatic. We attribute this to the combination of high atmospheric deposition (10–12 kg Cl ha^{-1} $year^{-1}$; National Atmospheric Deposition Program, 2017) and high evaporative enrichment in Florida (mean ratio of annual runoff to annual precipitation across sites is 0.22), leading to large aquifer Cl and Na mass. The large mass of seawater-derived evaporative solutes coupled to low topographic relief leads to long transit times that enhance chemostatic behaviour and also augment concentrations via substantial evaporative enrichment.

We observed strong support for the prediction that TOC enriches with increasing discharge across all catchments, supporting previous research from other regions (e.g., Bishop et al., 2004). The simple mechanistic explanation invoked for pH dilution may also explain the consistent positive β for C–Q associations across sites. In short, an expanding source area with increased discharge episodically connects regions where TOC accumulates (e.g., wetlands) with downstream waters. As with pH, higher flows from shallower source areas enhance interactions with regions of the catchment rich in organic carbon and respired CO_2.

Our results also support the hypothesis that nutrient (NO_3, TKN, PO_4, and TP) C–Q relationships are highly variable across catchments but centred on chemostasis. This variability was most evident for N species whose $|\beta|$ could exceed 1, whereas P species were more constrained ($-0.42 < \beta < 0.78$). For example, both Bowlegs Creek (02295013) and the Alapaha River (02317620) exhibited nearly ideal dilution behaviour for NO_3 ($\beta = -1.17$ and -0.71, respectively), but Orange Creek (02243000) and the Ocklawaha River (02240000) exhibited nearly ideal enriching behaviour for NO_3 ($\beta = 1.02$ and 1.25, respectively). Similarly, TKN β could be as low as −1.00 (Black Water Creek, 02235200), but as high as 1.48 (Santa Fe River, 02322800). Unusually low β values for TKN, like those observed at Black Water Creek, were particularly surprising because TKN typically tracked TOC enrichment behaviour across sites. Decoupling of TOC and TKN behaviour at sites with low TKN β values may indicate that ammonium dilution is stronger than organic N (and organic C) enrichment. Additionally, observations of enriching responses ($\beta > 0.2$) for PO_4/TP in 20% of P C–Q relationships contrast strong evidence of PO_4 dilution in two small coastal plain catchments (Hensley, McLaughlin, Cohen, & Decker, 2017). Overall, however, broad evidence for nutrient chemostasis suggests transport limitation despite a prevailing narrative that these two elements are under strong biotic control, and are thus preferentially retained on the landscape. We note that solutes under the strongest human influence were the only ones to exhibit enrichment responses (i.e., PO_4, NO_3, TP, TKN, and TOC; Figure 2a).

4.2 | Controls on C–Q relationships

although many studies have characterized C–Q relationships across watershed sizes, few have explicitly explored controls on these

relationships (but see Musolff et al., 2017). Our hypothesis that dominant controls included watershed size, land cover, and lithology was not well supported, supporting results from Godsey et al. (2009). Despite rejecting their control on the shape of C–Q relationships (i.e., β), we did observe consistent effects of watershed size on CV_C:CV_Q and strong influences of land cover and geology on FWCs. This generally suggests that land cover and watershed geology control the magnitude of solute sources, but not necessarily the modes and temporal dynamics of solute delivery.

4.2.1 | Lithology

We observed strong evidence of lithologic controls on C–Q relationships. As predicted, presence of P-rich Hawthorn Group sediments was significantly correlated with higher FWCs of TP and PO_4, and also with reduced concentration variation, suggesting that the Hawthorn acts as a relevant, and perhaps dominant, source of phosphorus to regional lakes (Cohen, Lamsal, Korhnak, & Long, 2008) and streams (Hensley et al., 2017). Similarly, Ca FWCs and presence/absence of limestone comported with expectations, with higher concentrations when carbonate exposure increases. Surprisingly, however, limestone presence led to greater Ca concentration variation relative to discharge (i.e., higher CV_C:CV_Q), possibly suggesting that local Ca supply to rivers is related to deeper weathering processes than implied by limestone surface outcroppings. Our 1% presence test for the Ocala formation, which exhibits extensive karst conduits that span multiple watersheds, may be inappropriate to measure the influence of this lithologic feature on C–Q relationships.

4.2.2 | Watershed size

Watershed size had little effect on β or FWC but had a strong influence on CV_C:CV_Q. However, the effect sign was opposite our expectations, which posited reduced solute variance with increasing watershed area because of cumulative sampling of heterogeneous source areas. On the contrary, CV_C:CV_Q increased with watershed size for every solute. This is largely due to a rapid decrease in flow variability with watershed size rather than increasing variability in solute concentration, which tends to remain constant across sizes. These findings are counter to expectations from other recent work at similar spatial scales that suggests convergence on TOC chemostasis with increasing stream order due to decreasing variability in solute concentrations that become dominated by instream and near-stream biogeochemical processes (Creed et al., 2015). Part of the explanation is that solutes and regions exhibit distinct and sometimes contrary behaviour. Clearly, to reconcile this contrary behaviour, large-scale pattern comparisons of C–Q relationships across solutes and ecoregions are still necessary.

Interestingly, FWC values of TOC and TKN decreased with drainage area in two watersheds where longitudinal comparisons were possible (Santa Fe River and Suwannee River; β_{TOC} = −0.48 and −0.70, respectively, and β_{TKN} = −0.30 and −0.29, respectively). This indicates how important headwater reaches are as organic solute sources, and how active the river network is for subsequent removal and dilution. It also contrasts results from mountainous lake chains where organic solutes increase along a lake catena (Sadro, Nelson, & Melack, 2012), potentially highlighting differences in lake and river behaviour. Notably, in those same two watersheds, FWCs for all other solutes (i.e., except TOC and TKN) increased with drainage area, supporting results from mountainous watersheds, where drainage area is associated with increasing geogenic solute concentrations (Frisbee, Phillips, Campbell, Liu, & Sanchez, 2011; Sadro et al., 2012). This pattern suggests similar outcomes of flow generation and solute availability in both coastal lowlands and mountainous terrain, where geogenic solute transport to streams and rivers increases along a river network.

4.2.3 | Land cover

Our results do not support significant land cover controls on the shape of C–Q relationships but instead indicate that land cover is common control on average solute concentrations of watersheds. The stark contrast in FWC relationships between urban cover and wetland/forest cover for all solutes (Table 4) suggests the importance of surface water storage on C–Q dynamics. Urban landscapes are typically associated with reduced surficial hydrologic storage due to impervious cover and wetland losses; this loss of storage increases the relative contribution of subsurface flows and associated geogenic solutes to streams. In contrast, greater wetland cover and forest cover enable distributed landscape storage and abstractions, decreasing the contribution of subsurface water to downstream waters and allowing for solute removal through biogeochemical processing. We also observed that wetland cover was associated with greater TOC and TKN FWC values, emphasizing the source role of wetlands for organic material (Gergel, Turner, & Kratz, 1999). Surprisingly, greater agriculture cover was not associated with nutrient chemostasis as we predicted, although it was associated with higher TP/PO_4 FWCs. The absence of chemostasis for nutrients may be explained by recent findings from Musolff et al. (2017) who suggest that the spatial structure of solute sources is the key determinant of β and CV_C:CV_Q. As such, it is possible that despite having overall greater nutrient mass across agricultural landscapes, these sources are still spatially heterogeneous, precluding catchment chemostasis.

Our temporal lens may also limit our analysis: Our land cover assessment considers only 2008–2010 and thus cannot account for land cover change. Because we did not attempt to match land cover dates with measured stream flow or chemistry, we effectively assume recent land cover change has been modest. In some areas, this is clearly invalid and may limit the specificity of our detected land cover controls on C–Q relationships; further work should account for historical land use changes, particularly where long time series of catchment responses are available (Van Meter, Basu, Veenstra, & Burras, 2016).

4.3 | Breakpoints

Our results raise important questions about the generality of power-law characterizations of C–Q relationships in rivers and streams. Notably, nutrient (NO_3, TP, and PO_4) concentrations frequently did not conform to power-law functions with discharge, exhibited large variability around the best fit line, or reversed fitted slope (β) sign at intermediate discharge. This departure from power-law behaviour

may suggest that processes less directly influenced by discharge variation (e.g., biological processes) meaningfully influence solute delivery. More likely, however, is that nutrient transport to streams is governed by activation of transient flowpaths, a process dependent on watershed saturation. This seems particularly salient in cases where β reverses sign (i.e., enrichment at low to intermediate flow; dilution at intermediate to high flow).

Three clear trends were evident from our breakpoint analysis: (a) across sites, breakpoints for all solutes centred on median flow; (b) within a site, breakpoints for all solutes were located near the same discharge; and (c) in most cases, slopes (β) decreased above the breakpoint discharge. These three properties suggest that regardless of low-flow solute behaviour, high-flow behaviour tends towards dilution, with high-flow similarly defined for all catchments as >50% flow exceedance. The apparent generality of slope breaks at median flow emerges from our synthesis and important recent work (Moatar et al., 2017). This generality suggests common solute and flow generation processes across divergent watersheds. Specifically, rates of weathering and transport are controlled by watershed discharge capacity, with median flow apparently defining a common threshold delimiting source limitation (enrichment or chemostasis) from transport limitation (dilution). Given that catchment morphology and flow generation exert reciprocal controls over long time scales, consistent median-flow breakpoints may be an emergent property of feedbacks between catchment flow and form.

Shifts to dilution behaviour above breakpoints indicate source limitation at higher flows. For Ca and Mg, breakpoints shifted from chemostasis to dilution, a common finding for catchments elsewhere (Moatar et al., 2017). The most notable downward shifts in β were for NO_3, where positive low-flow β values became negative above the breakpoint. This behaviour was mostly confined to NO_3 and may result from dilution of nitrate sources that exhibit extremely stable flow (e.g., Florida's many artesian springs; Heffernan et al., 2010). This explanation differs from Moatar et al. (2017), who found similar patterns, but suggests that they result from biogeochemical controls. Specifically, they contend that low flows favour biotic NO_3 uptake; but as discharge increases, the uptake velocity dramatically declines, precluding clear impacts on NO_3 flux. Although this is plausible, particularly where denitrification is the principal mode of retention (assimilated N is rapidly remineralized, precluding a clear network role in N retention), we reason that because NO_3 is so mobile, it is generally depleted from the upper soil profiles from which high flows are sourced. Indeed, in our study area, most nitrate is in deep groundwater (not soil water), suggesting slope breaks at median flow mark the onset of shallow flowpaths that overwhelm flows sourced from the deeper NO_3-rich pool.

We also observed slope breaks for TOC at many sites, where steep low-flow β values get shallower at higher flows. This indicates activation of source zones at intermediate flows. The low-flow behaviour (i.e., enrichment with flow) supports the contention that episodically connected wetlands, the time dynamics of which vary dramatically across the array of wetlands in the landscape, regulate carbon export at local and watershed scales. Most TOC breakpoints were "up-flat" (i.e., enriching-chemostatic) as opposed to "flat-up" (i.e., chemostatic-enriching) dissolved organic carbon breakpoints observed in Moatar et al. (2017) (we note that the vast majority of TOC in our study rivers is present as dissolved organic carbon). This difference may suggest variation in source locations, and modes of mobilization. In our setting, water from high TOC sources mobilizes with even modest flow changes, but these effects saturate once the landscapes wetlands are surface connected. In contrast, in the higher relief catchments in Moatar et al. (2017), high flow is required to activate floodplain connections and thus high TOC sources.

Increases in β after the breakpoint were primarily associated with TP. This upward "v" C–Q curve may arise from mobilization of P from interstitial waters in bed sediments at high flow, as well as sediment-bound P suspended during high flows and impacting streamwater P via desorption. Riparian fluxes of P from floodplain soils may further enhance this effect when previously immobile floodplain P pools (Noe & Hupp, 2005) mobilize at high flows. Clockwise hysteresis observed in between C and Q during storms in similar coastal plain watersheds (Hensley et al., 2017) reinforces the notion that proximate sources of P mobilized under rising discharge conditions are important to our observed C–Q breakpoint patterns.

Several recent studies have visually documented C–Q breakpoints (e.g., Meybeck & Moatar, 2012; Moatar et al., 2017) and argued that they occur near median flow. Our methods empirically estimate breakpoint positions and strongly reinforce the observation that most centre on 50% flow exceedance probability; we also observed substantial unexplained variability about this value of interest in refining our understanding of the origins of this signal. That we observed a similar array and preponderance of C–Q modalities (i.e., changes in β at the breakpoint) as recent comprehensive work (Meybeck & Moatar, 2012, Moatar et al., 2017) implies that simple power-law C–Q relationships may be the exception, not the norm. Commonalities in C–Q modalities among our southeastern U.S. study sites and the French sites in Moatar et al. (2017) indicate that scaling breaks are global, but generally overlooked, feature of catchments.

4.3.1 | Consequences of breakpoints in the C–Q relationship

Previous studies show clear C–Q breakpoints or nonideal power-law behaviour (e.g., Baronas, Torres, Clark, & Joshua, 2017; Clow & Mast, 2010; Godsey et al., 2009; Herndon et al., 2015b; Smith et al., 1996) but tend to overlook the implications of these breakpoints. For example, Clow and Mast (2010) show a breakpoint that shifts the silica C–Q slope from −0.1 to near dilution (−1), implying that although chemostasis dominates at low flows, dilution is a better description at high flows. Despite this break, the authors use an overall C–Q slope of −0.12. We argue that it is likely possible that chemostatic behaviour predominantly observed in the literature is mostly present under low flows. Because most solute flux occurs at high flows (e.g., Jawitz & Mitchell, 2011), loads predicted on the assumption of chemostatic conditions may be dramatically incorrect.

A trivial comparison of loads estimated with a chemostatic C–Q relationship (i.e., $\beta = 0$) to loads estimated from a C–Q relationship described as chemostatic in the literature (e.g., $\beta = 0.1$) results in substantially different estimates. This is well vetted in the literature, with predictions based on rating curves with high variability substantially underpredicting actual fluxes (e.g., Horowitz, 2003; Walling & Webb, 1988). As such, chemostatic assumptions result in erroneous load calculations unless

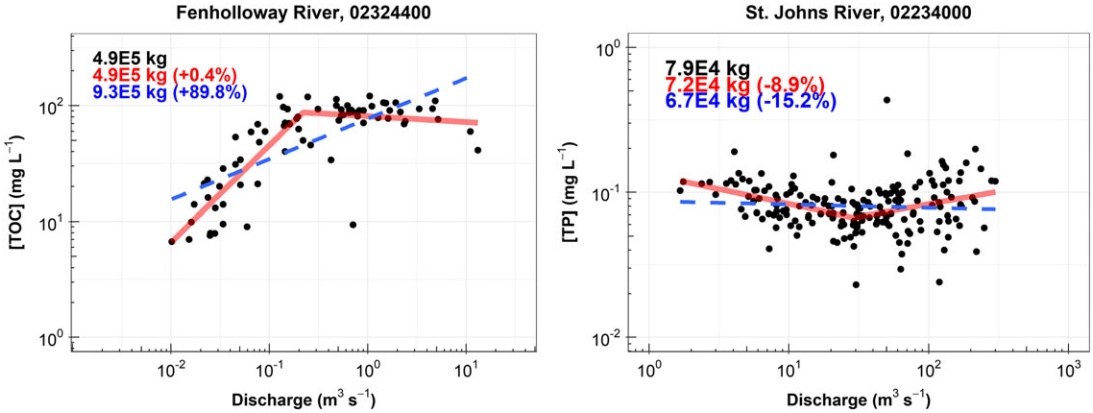

FIGURE 5 Example comparison of constant power-law relationship (blue, dashed line) for C–Q versus breakpoint power-law relationship (red, solid line) for two select sites and two select solutes within those sites. We calculate regression-estimated loads for directly measured discharge values (i.e., discharge values at black points) and compare the sum of these estimated loads to the sum of directly measured loads from C–Q data (black points). Coloured numbers in the upper-left corner of graphs indicate calculated load sums for data points (black) and estimated load sums for the two different power-law relationships types. Parenthetical numbers indicate percentage differences from directly measured loads (black data points). TOC = total organic carbon; TP = total phosphorus

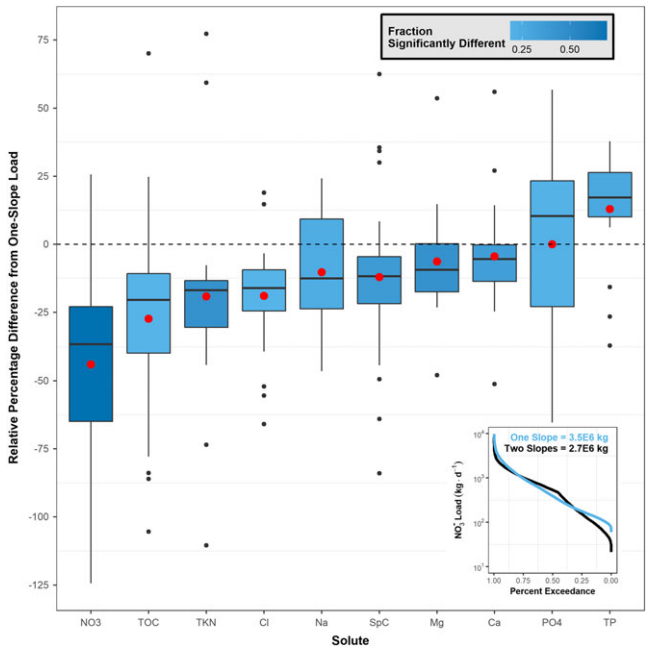

FIGURE 6 Relative percentage differences between the sum of loads from a load duration curve for loads calculated from the breakpoint power-law model and the one-slope power-law model. Results are arranged by solute and compared across sites. Boxplots are filled according to the fraction of C–Q relationships that had breakpoints where breakpoint models provided a significantly different load estimate than did one-slope models across the load duration curve (*t* test). Red points indicate means of distributions. The inset shows an example load duration curve comparison for NO_3 at the Withlacoochee River (02319000). Numbers in the top right of the inset are total load sums from the load duration curves. SpC = specific conductance; TKN = total Kjeldahl nitrogen; TOC = total organic carbon; TP = total phosphorus

operationally defined chemostatic relationships are indeed chemostatic and homoscedastic and have low variance. Our breakpoint analysis adds an additional layer for consideration: There are consequences of assuming chemostasis as well as using a single power-law to describe concentration variation with discharge (Figure 5). Although there are numerous methods to estimate loads, including composite methods that use residual corrections to reduce bias in simple regression analysis (e.g., Appling, Leon, & McDowell, 2015), we use simple linear log(C)–log(Q) regression models (i.e., with and without breakpoints) to determine our estimated loads (Figure 5) and show significant deviations from these loads when breakpoints are considered.

To determine the extent of variability in load estimation from breakpoint and nonbreakpoint C–Q relationships, we calculated loads for all sites with both types of relationships using a load duration curve approach. Loads calculated from these two approaches were significantly different ($\alpha = 0.05$) for 20–70% of catchments and solutes (Figure 6). In general, where β values decline above median flow, loads are substantially overestimated, with nitrate and TOC overestimated by as much as 125%. Likewise, β values that increase above median flow, as was generally observed for phosphorus, lead to load underestimates by as much as 57%.

We suggest researchers critically evaluate the use of simple power-law models for C–Q relationships when estimating loads. Future work should focus on model development that is able to mechanistically explain scaling break behaviour seen for nearly all solutes in this study.

ACKNOWLEDGMENTS

We acknowledge financial support from the National Council for Air and Stream Improvement, the Florida Forest Service, and the National Institute of Food and Agriculture (NIFA) via CRIS project FLA-FOR-005284.

ORCID

Jacob S. Diamond http://orcid.org/0000-0002-5392-5707

REFERENCES

Alexandre, A., Meunier, J. D., Colin, F., & Koud, J. M. (1997). Plant impact on the biogeochemical cycle of silicon and related weathering processes. *Geochimica et Cosmochimica Acta*, *61*(3), 677–682.

Ameli, A., Beven, K., Erlandsson, M., Creed, I., McDonnell, J. J., & Bishop, K. (2016). Primary weathering rates, water transit times, and concentration–discharge relations: A theoretical analysis for the critical zone. *Water Resources Research*.

Anderson, S. P., Dietrich, W. E., Torres, R., Montgomery, D. R., & Loague, K. (1997). Concentration–discharge relationships in runoff from a steep, unchanneled catchment. *Water Resources Research*, *33*(1), 211–225.

Appling, A. P., Leon, M. C., & McDowell, W. H. (2015). Reducing bias and quantifying uncertainty in watershed flux estimates: The R package loadflex. *Ecosphere*, *6*(12), 1–25.

Baronas, J. J., Torres, M. A., Clark, K. E., & Joshua, A. (2017). Mixing as a driver of temporal variations in river hydrochemistry. Part 2: Major and trace element concentration dynamics in the Andes–Amazon transition. *Water Resources Research*. https://doi.org/10.1002/2016WR019729

Basu, N. B., Destouni, G., Jawitz, J. W., Thompson, S. E., Loukinova, N. V., Darracq, A., … Rao, P. S. C. (2010). Nutrient loads exported from managed catchments reveal emergent biogeochemical stationarity. *Geophysical Research Letters*, *37*. https://doi.org/10.1029/2010GL045168

Basu, N. B., Thompson, S. E., & Rao, P. S. C. (2011). Hydrologic and biogeochemical functioning of intensively managed catchments: A synthesis of top-down analyses. *Water Resources Research*, *47*. https://doi.org/10.1029/2011WR010800

Beven, K. J. (2010). Preferential flows and travel time distributions: Defining adequate hypothesis tests for hydrological process models. *Hydrological Processes*, *24*(12), 1537–1547.

Bishop, K., Seibert, J., Kohler, S., & Laudon, H. (2004). Resolving the double paradox of rapidly mobilized old water with highly variable responses in runoff chemistry. *Hydrological Processes*, *18*, 185–189.

Botter, G., Bertuzzo, E., & Rinaldo, A. (2010). Transport in the hydrologic response: Travel time distributions, soil moisture dynamics, and the old water paradox. *Water Resources Research*, *46*(3).

Brantley, S. L. (2008). Kinetics of mineral dissolution. In *Kinetics of water–rock interaction* (pp. 151–210). New York: Springer.

Clauset, A., Shalizi, C. R., & Newman, M. E. (2009). Power-law distributions in empirical data. *SIAM Review*, *51*(4), 661–703.

Clow, D. W., & Drever, J. I. (1996). Weathering rates as a function of flow through an alpine soil. *Chemical Geology*, *132*, 131–141.

Clow, D. W., & Mast, M. A. (2010). Mechanisms for chemostatic behavior in catchments: Implications for CO2 consumption by mineral weathering. *Chemical Geology*, *269*(1), 40–51.

Cohen, M. J., Lamsal, S., Korhnak, L., & Long, L. (2008). Spatial nutrient loading and sources of phosphorus in the Newnans Lake watershed. SJRWMD report SJ2008-SP29.

Conley, D. J. (2002). Terrestrial ecosystems and the global biogeochemical silica cycle. *Global Biogeochemical Cycles*, *16*(4).

Creed, I. F., McKnight, D. M., Pellerin, B. A., Green, M. B., Bergamaschi, B. A., Aiken, G. R., … Stackpoole, S. M. (2015). The river as a chemostat: Fresh perspectives on dissolved organic matter flowing down the river continuum. *Canadian Journal of Fisheries and Aquatic Sciences*, *72*(8), 1272–1285.

Epstein, E. (1994). The anomaly of silicon in plant biology. *Proceedings of the National Academy of Sciences*, *91*(1), 11–17.

Evans, C., & Davies, T. D. (1998). Causes of concentration/discharge hysteresis and its potential as a tool for analysis of episode hydrochemistry. *Water Resources Research*, *34*(1), 129–137.

Feng, X., Kirchner, J. W., & Neal, C. (2004). Spectral analysis of chemical time series from long-term catchment monitoring studies: Hydrochemical insights and data requirements. *Water, Air, and Soil Pollution*, *4*, 221–235.

Frisbee, M. D., Phillips, F. M., Campbell, A. R., Liu, F., & Sanchez, S. A. (2011). Streamflow generation in a large, alpine watershed in the southern Rocky Mountains of Colorado: Is streamflow generation simply the aggregation of hillslope runoff responses? *Water Resources Research*, *47*. https://doi.org/10.1029/2010WR009391

Gergel, S. E., Turner, M. G., & Kratz, T. K. (1999). Dissolved organic carbon as an indicator of the scale of watershed influence on lakes and rivers. *Ecological Applications*, *9*(4), 1377–1390.

Godsey, S. E., Aas, W., Clair, T. A., de Wit, H. A., Fernandez, I. J., Kahl, J. S., … Kirchner, J. W. (2010). Generality of fractal 1/f scaling in catchment tracer time series, and implications for catchment travel time distributions. *Hydrological Processes*, *24*, 1660–1671.

Godsey, S. E., Kirchner, J. W., & Chow, D. W. (2009). Concentration–discharge relationships reflect chemostatic characteristics of US catchments. *Hydrological Processes*, *23*, 1844–1864.

Guan, K., Thompson, S. E., Harman, C. J., Basu, N. B., Rao, P. S. C., Sivapalan, M., … Kalita, P. K. (2011). Spatiotemporal scaling of hydrological and agrochemical export dynamics in a tile-drained Midwestern watershed. *Water Resources Research*, *47*. https://doi.org/10.1029/2010WR009997

Heffernan, J. B., Cohen, M. J., Frazer, T. K., Thomas, R. G., Rayfield, T. J., Gulley, J., … Graham, W. D. (2010). Hydrologic and biotic influences on nitrate removal in a subtropical spring-fed river. *Limnology and Oceanography*, *55*(1), 249–263.

Hensley, R. T., McLaughlin, D. L., Cohen, M. J., & Decker, P. H. (2017). Stream phosphorus dynamics of minimally impacted coastal plain watersheds. *Hydrological Processes*.

Herndon, E. M., Dere, A. L., Sullivan, P. L., Norris, D., Reynolds, B., & Brantley, D. S. L. (2015a). Biotic controls on solute distribution and transport in headwater catchments. *Hydrologic and Earth Systems Science Discussions*, *12*, 213–243.

Herndon, E. M., Dere, A. L., Sullivan, P. L., Norris, D., Reynolds, B., & Brantley, S. L. (2015b). Landscape heterogeneity drives contrasting concentration–discharge relationships in shale headwater catchments. *Hydrology and Earth Science Systems*, *19*, 3333.

Horowitz, A. J. (2003). An evaluation of sediment rating curves for estimating suspended sediment concentrations for subsequent flux calculations. *Hydrological processes*, *17*(17), 3387–3409.

Jawitz, J. W., & Mitchell, J. (2011). Temporal inequality in catchment discharge and solute export. *Water Resources Research*, *47*. https://doi.org/10.1029/2010WR010197

Johnson, N. M., & Likens, G. E. (1969). A working model for the variation in stream water chemistry at the Hubbard Brook Experimental Forest, New Hampshire. *Water Resources Research*, *5*(6), 1353–1363.

Kim, H., Dietrich, W. E., Thurnhoffer, B. M., Bishop, J. K., & Fung, I. Y. (2017). Controls on solute concentration–discharge relationships revealed by simultaneous hydrochemistry observations of hillslope runoff and stream flow: The importance of critical zone structure. *Water Resources Research*. https://doi.org/10.1002/2016WR019722

Kirchner, J. W., Feng, X., Neal, C., & Robson, D. A. J. (2004). The fine structure of water-quality dynamics: The (high-frequency) wave of the future. *Hydrological Processes*, *18*, 1353–1359.

Kurz, M. J., de Montety, V., Martin, J. B., Cohen, M. J., & Foster, C. R. (2013). Controls on diel metal cycles in a biologically productive carbonate-dominated river. *Chemical Geology*, *358*, 61–74. https://doi.org/10.1016/j.chemgeo.2013.08.042

Li, L., Bao, C., Sullivan, P. L., Brantley, S., Shi, Y., & Duffy, C. (2017). Understanding watershed hydrogeochemistry: 2. Synchronized hydrological and geochemical processes drive stream chemostatic behavior. *Water Resources Research*. https://doi.org/10.1002/2016WR018935

Meybeck, M., & Moatar, F. (2012). Daily variability of river concentrations and fluxes: Indicators based on the segmentation of the rating curve. *Hydrological Processes*, *26*(8), 1188–1207.

Moatar, F., Abbott, B. W., Minaudo, C., Curie, F., & Pinay, G. (2017). Elemental properties, hydrology, and biology interact to shape concentration–discharge curves for carbon, nutrients, sediment, and major ions. *Water Resources Research*. https://doi.org/10.1002/2016WR019635

Mulholland, P. J., & Hill, W. R. (1997). Seasonal patterns in streamwater nutrient and dissolved organic carbon concentrations: Separating catchment flow path and in-stream effects. *Water Resources Research*, *33*(6), 1297–1306.

Murphy, J. C., Hornberger, G. M., & Liddle, R. G. (2012). Concentration–discharge relationships in the coal mined region of the New River basin and Indian Fork sub-basin, Tennessee, USA. *Hydrological Processes*. https://doi.org/10.1002/hyp.9603

Musolff, A., Fleckenstein, J. H., Rao, P. S. C., & Jawitz, J. W. (2017). Emergent archetype patterns of coupled hydrologic and biogeochemical responses in catchments. *Geophysical Research Letters*, *44*, 4143–4151. https://doi.org/10.1002/2017GL072630

Musolff, A., Schmidt, C., Selle, B., & Fleckenstein, J. H. (2015). Catchment controls on solute export. *Advances in Water Resources*, *86*, 133–146.

Nangia, S., & Garrison, B. J. (2008). Reaction rates and dissolution mechanisms of quartz as a function of pH. *The Journal of Physical Chemistry A*, *112*(10), 2027–2033.

National Atmospheric Deposition Program (NRSP-3). (2017). NADP Program Office, Illinois State Water Survey, University of Illinois, Champaign, IL 61820.

Noe, G. B., & Hupp, C. R. (2005). Carbon, nitrogen, and phosphorus accumulation in floodplains of Atlantic coastal plain rivers, USA. *Ecological Applications*, *15*(4), 1178–1190.

Pearce, A. J., Stewart, M. K., & Sklash, M. G. (1986). Storm runoff generation in humid headwater catchments: 1. Where does the water come from? *Water Resources Research*, *22*(8), 1263–1272.

Pellerin, B. A., Bergamaschi, B. A., Gilliom, R. J., Crawford, C. G., Saraceno, J., Frederick, C. P., & Murphy, J. C. (2014). Mississippi River nitrate loads from high frequency sensor measurements and regression-based load estimation. *Environmental Science & Technology*, *48*(21), 12612–12619.

R Core Team (2016). *R: A language and environment for statistical computing*. Vienna, Austria: R Foundation for Statistical Computing URL: https://www.r-project.org/

Sadro, S., Nelson, C. E., & Melack, J. M. (2012). The influence of landscape position and catchment characteristics on aquatic biogeochemistry in high-elevation lake-chains. *Ecosystems*, *15*(3), 363–386.

Seibert, J., Grabs, T., Köhler, S., Laudon, H., Winterdahl, M., & Bishop, K. (2009). Linking soil-and stream-water chemistry based on a riparian flow-concentration integration model. *Hydrology and Earth System Sciences*, *13*(12), 2287–2297.

Smith, S. V., Chambers, R. M., & Hollibaugh, J. T. (1996). Dissolved and particulate nutrient transport through a coastal watershed–estuary system. *Journal of Hydrology*, *176*(1–4), 181–203.

Stallard, R. F., & Murphy, S. F. (2014). A unified assessment of hydrologic and biogeochemical responses in research watersheds in eastern Puerto Rico using runoff–concentration relations. *Aquatic Geochemistry*, *20*(2–3), 115–139.

Thompson, S. E., Basu, N. B., Lascurain, J., Aubeneau, A., & Rao, P. S. C. (2011). Relative dominance of hydrologic versus biogeochemical factors on solute export across impact gradients. *Water Resources Research*, *47*(10).

Van Meter, K. J., Basu, N. B., Veenstra, J. J., & Burras, C. L. (2016). The nitrogen legacy: Emerging evidence of nitrogen accumulation in anthropogenic landscapes. *Environmental Research Letters*, *11*(3), 035014.

Vito, M., & Muggeo, R. (2003). Estimating regression models with unknown break-points. *Statistics in Medicine*, *22*, 3055–3071.

Vito, M., & Muggeo, R. (2008). Segmented: An R package to fit regression models with broken-line relationships. R News, 8/1, 20-25. URL http://cran.r-project.org/doc/Rnews/

Walling, D. E., & Webb, B. W. (1988). *The reliability of rating curve estimates of suspended sediment yield: Some further comments. Sediment budgets* (Vol. 174). IAHS Publication.

Watershed Boundary Dataset for Florida. (2012). Available URL: http://datagateway.nrcs.usda.gov, Accessed 01/08/2012.

How to cite this article: Diamond JS, Cohen MJ. Complex patterns of catchment solute–discharge relationships for coastal plain rivers. *Hydrological Processes*. 2018;32:388–401. https://doi.org/10.1002/hyp.11424